

# Simulation Research on Forward Problem of Magnetoacoustic Concentration Tomography of Magnetic Nanoparticles with Magnetic Induction Based on Multi-Coils

Xiaoheng Yan\*, Peng Gao, Mingchen Cai, and Zhengxing Li

**Abstract**—Magnetoacoustic concentration tomography of magnetic nanoparticles (MNPs) with magnetic induction (MACT-MI) is a multi-physics field imaging method based on the coupling effect of magnetic field and acoustic field. In order to generate a gradient magnetic field with higher uniformity by using lower current excitation, this paper takes the magnetic field gradient of 0.3 T/m as the design objective and utilizes the Beetle Antennae Search Algorithm to optimize the parameters of the excitation current of multiple coils. The uniformity of gradient magnetic field generated by four typical six-coils structures with different radii and distances was compared with that generated by the Maxwell coil, and then the optimal structure of six-coils was determined. By using the finite element method, the physical process of MACT-MI was numerically solved according to the optimization results, and we obtained the one-dimensional and two-dimensional distribution images of magnetic force and sound pressure. The results show that compared with the Maxwell coil, the multi-coil structure can effectively reduce the current excitation and provide a higher uniform gradient magnetic field, which makes the magnetic force of MNPs more uniform and promotes the complete reconstruction of the sound source. These research results can provide research ideas for the optimization of MACT-MI system and lay a foundation for subsequent experiments and even clinical practice.

## 1. INTRODUCTION

With the rapid development of micro and nanoparticles technologies, the application of magnetic nanomaterials in molecular imaging has also attracted extensive attention of researchers [1–3]. Magnetic particle imaging, a tracer-based imaging method, has important clinical value for reflecting pathological and physiological changes. Scholars from many countries have competed in research on magnetic particle imaging. As early as 2006, Oh et al. showed that magnetic force excited ultrasound imaging is an imaging modality to identifying tissue macrophages containing magnetic superparamagnetic iron oxide SPIO nanoparticles [4]. In order to improve the sensitivity and signal-to-noise, Mehrmohammadi et al. in 2011 used super paramagnetic nanoscale arrays to enhance pulsed magneto-motive ultrasound imaging. Larger clusters of magnetic nanoparticles were subjected to greater magnetic force, and the measured ultrasonic signal was stronger [5]. In 2012, Hu and He obtained the boundary images of magnetic nanoparticles embedded in biological tissues by using microsecond pulse magnetic simulation with good imaging sensitivity and resolution [6]. In 2015, Bringout and Buzug proposed an electromagnetic coil design method for magnetic particle imaging scanners and verified cylindrical driving coil by numerical calculation, demonstrating that it is possible to optimize the scanner design and improve imaging capabilities using this technique [7]. In 2018, Yan et al. studied the influence of magnetic

---

*Received 31 May 2021, Accepted 13 September 2021, Scheduled 24 September 2021*

\* Corresponding author: Xiaoheng Yan (xiaohengyan@163.com).

The authors are with the Faculty of Electrical and Control Engineering, Liaoning Technical University, Huludao 125105, Liaoning, China.

nanoparticles on magnetoacoustic imaging, and the research results showed that magnetic nanoparticles could generate large sound pressure signals with more uniform distribution of sound pressure [8]. In 2019, Hamanaga et al. used a combination of field-free lines and multiple pickup coils to conduct the three-dimensional detection of magnetic nanoparticles samples and discussed how the imaging quality decreased when the gradient magnetic field was reduced [9]. In 2020, Shi et al. proposed a magnetoacoustic concentration tomography of magnetically induced magnetic nanoparticles (MACT-MI), which proved that this method could detect and reconstruct the concentration of magnetic nanoparticles in biological tissues [10]. In the same year, Yan et al. proposed a reconstruction algorithm of the MACT-MI inverse problem based on the method of moments, which used different shape models to reconstruct the image of the sound source and the concentration of superparamagnetic nanoparticles [11].

At present, in order to improve the image reconstruction effect of magnetoacoustic imaging, some scholars have studied MNPs characteristics, pulse signal form, signal acquisition method, image reconstruction algorithm, and other aspects. In view of this, in order to reduce the current excitation and to build a higher uniformity gradient magnetic field, we use the Beetle Antennae Search algorithm to optimize the excitation current of the multi-coils. The gradient magnetic field generated by the multi-coil structure is compared and studied. We analyze the magnetic force generated by multiple coils and the Maxwell coil acting on target sample. The physical process of sound pressure signal generated by target sample is studied.

## 2. IMAGING PRINCIPLE

The basic principle of MACT-MI is shown in Fig. 1. A time-varying magnetic field is generated by a Maxwell coil fed with alternating current pulse in the opposite direction, and the target sample labeled by MNPs is placed in the time-varying magnetic field. MNPs vibrate under the action of magnetic force in the time-varying magnetic field, and then emit ultrasonic wave. An ultrasonic transducer is used to receive the sound pressure signal, and the concentration distribution image of MNPs is reconstructed by time inversion method and finite difference method.

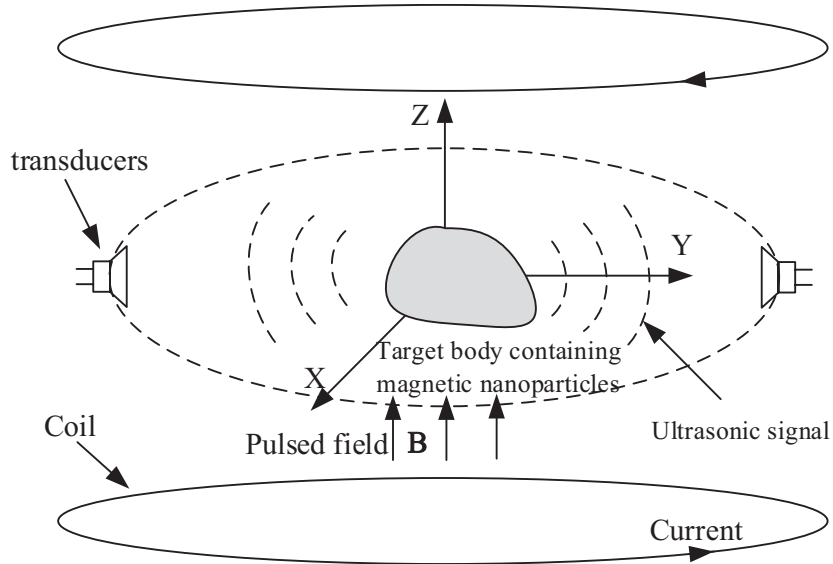


**Figure 1.** Schematic diagram of MACT-MI.

In the MACT-MI positive problem, MNPs generate ultrasonic signals excited by mechanical vibration under the action of time-varying magnetic force. When an external gradient magnetic field is applied in the  $z$  direction, the magnetic force density  $\mathbf{F}$  can be described as [10]

$$\mathbf{F} = N \frac{m^2}{3kT} B_z \frac{\partial B_z}{\partial z} \mathbf{e}_z \quad (1)$$

where  $N$  is the number of MPNs in unit volume,  $m$  the magnitude of inherent magnetic moment,  $k$  the Boltzmann constant, and  $T$  the absolute temperature.

In actual experiments, the magnetoacoustic signal generated by MNPs vibration is weak, and the main reason is that the magnetic force of MNPs is too small to send out strong enough magnetoacoustic signal. It can be seen from Equation (1) that the magnitude of magnetic force is determined by the properties of MNPs and the gradient of external magnetic field  $\frac{\partial B_z}{\partial z}$ . Therefore, when the material properties of MNPs are constant, the multi-coil structure can provide a larger external magnetic field gradient by using small current excitation, which plays an important role in increasing the force of MNPs and enhancing the magneto-acoustic signal.

In the imaging region, the Maxwell coil can generate gradient magnetic field with good uniformity and wide uniform area [12, 13], but in order to obtain gradient magnetic field with higher uniformity in the imaging region, it needs to meet the requirements

$$\left. \frac{\partial^2 B_z}{\partial z^2} \right|_{z=Z_0} = \left. \frac{\partial^3 B_z}{\partial z^3} \right|_{z=Z_0} = \dots = \left. \frac{\partial^n B_z}{\partial z^n} \right|_{z=Z_0} \equiv 0. \tag{2}$$

Obviously, the Maxwell coil does not satisfy this equation. In order to obtain highly uniform gradient magnetic field, multi-coil structure can be used to achieve this [14–16]. Fig. 2 shows four typical 6-coil structures [14–16]. In combination with Formula (2), we can get the magnetic field whose lowest non-zero derivative is the 13th order by selecting radius  $R$ , the distance between coils  $a$  and the current  $I$ , so that we can obtain the gradient magnetic field with better uniformity, and thus obtain the equations.

$$\begin{cases} I_1 \left. \frac{d^5 B_z}{dz^5} \right|_{z=d1} + I_2 \left. \frac{d^5 B_z}{dz^5} \right|_{z=d2} + I_3 \left. \frac{d^5 B_z}{dz^5} \right|_{z=d3} = 0 \\ I_1 \left. \frac{d^7 B_z}{dz^7} \right|_{z=d1} + I_2 \left. \frac{d^7 B_z}{dz^7} \right|_{z=d2} + I_3 \left. \frac{d^7 B_z}{dz^7} \right|_{z=d3} = 0 \\ I_1 \left. \frac{d^9 B_z}{dz^9} \right|_{z=d1} + I_2 \left. \frac{d^9 B_z}{dz^9} \right|_{z=d2} + I_3 \left. \frac{d^9 B_z}{dz^9} \right|_{z=d3} = 0 \\ I_1 \left. \frac{d^{11} B_z}{dz^{11}} \right|_{z=d1} + I_2 \left. \frac{d^{11} B_z}{dz^{11}} \right|_{z=d2} + I_3 \left. \frac{d^{11} B_z}{dz^{11}} \right|_{z=d3} = 0 \end{cases} \tag{3}$$

Under the excitation of gradient magnetic field, the sound field excited by MNPs can be calculated by using the linear active sound pressure wave equation. The equation and initial conditions can be expressed as [10]

$$\nabla^2 p(\mathbf{r}, t) - \frac{1}{c_s^2} \frac{\partial^2 p(\mathbf{r}, t)}{\partial t^2} = \nabla \cdot f(\mathbf{r}, t) \tag{4}$$

$$\begin{cases} p|_{t=0} = 0 \\ \left. \frac{\partial p}{\partial t} \right|_{t=0} = 0 \end{cases} \tag{5}$$

In this equation,  $\mathbf{r}$  is any point in space,  $p(\mathbf{r}, t)$  the spatial and temporal distribution of the sound pressure field,  $c_s$  the speed of sound in biological tissue,  $f(\mathbf{r}, t)$  the magnetic force received by MNPs, magnetic divergence from  $\nabla \cdot f(\mathbf{r}, t)$  the sound source term, and the boundary conditions are shown in Formula (5).

### 3. SIMULATION RESEARCH

#### 3.1. Simulation Study of Magnetic Field Gradient

According to the characteristics of different coil structures, different multi-coil structures can be obtained by adjusting the spacing  $a$  and radius  $R$ . Take parameters  $R1 = R2 = R3$ ,  $R1 < R2 < R3$ ,  $R1 > R2 > R3$ , and  $a1 = a2 = a3$ , respectively, four structures composed of six coils are obtained, as shown in Fig. 2.

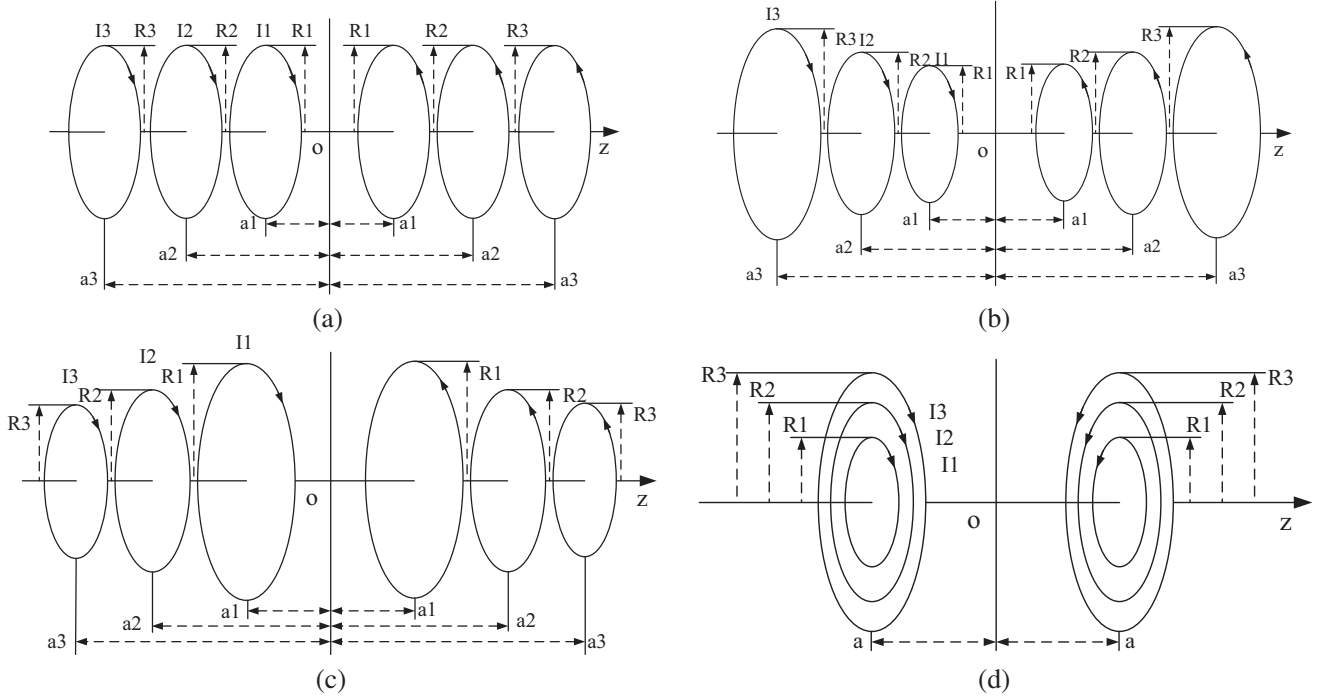


**Figure 2.** The structure of 6 coils under different parameters. (a)  $R1 = R2 = R3$ . (b)  $R1 < R2 < R3$ . (c)  $R1 > R2 > R3$ . (d)  $a1 = a2 = a3$ .

In this paper, the Beetle Antennae Search algorithm [17, 18] is used to optimize the current values of the four types of six-coils structures and Maxwell coils as shown in Fig. 2. The non-uniformity value  $\delta$  was used to measure the uniformity of the gradient magnetic field [19].

$$\delta = \sum \frac{\left| \frac{\partial B_z}{\partial z} - \frac{\partial B_{zset}}{\partial z} \right|}{\frac{\partial B_{zset}}{\partial z}} \quad (6)$$

The fitness function is established according to Equation (6). The points within the gradient magnetic field in the target area are uniformly sampled, and the target value is compared with the actual value to obtain the fitness function

$$Fitness = \sum_{i=1}^M \frac{|G_{Zi}(I_1, I_2, \dots, I_n) - G_{Zset}|}{G_{Zset}} \quad (7)$$

*s.t.*  $-I_{max} \leq I_j \leq I_{max}$

where  $I_j$  is the current of the  $J$ th coil,  $n$  the number of coils,  $M$  the number of reference points selected in the imaging area,  $G_{Zi}$  the magnetic field gradient in the  $z$  direction at the  $i$ th reference point, and  $G_{Zset}$  the target magnetic field gradient in the  $z$  direction set. In the constraint condition,  $I_{max}$  is the maximum current value set. The optimization process is shown in Figure 3.

According to the Beetle Antennae Search algorithm, Matlab and Comsol software were used for co-simulation. Taking 0.3 T/m as the target magnetic field gradient, the coefficient between the two whiskers and the step size was set as 5; the distance between the two whiskers was 0.1; the initial step size was 10; the step size attenuation coefficient was 0.95; and the number of iterations was 300. The variation range of current value is [0, 300] A.

The optimized coil current and fitness function values are shown in Table 1. When the magnetic field gradient of 0.3 T/m is generated in the imaging region, the current excitation required by the Maxwell coil is 241 A, and the current excitation required by the multi-coil structure is between 100 A

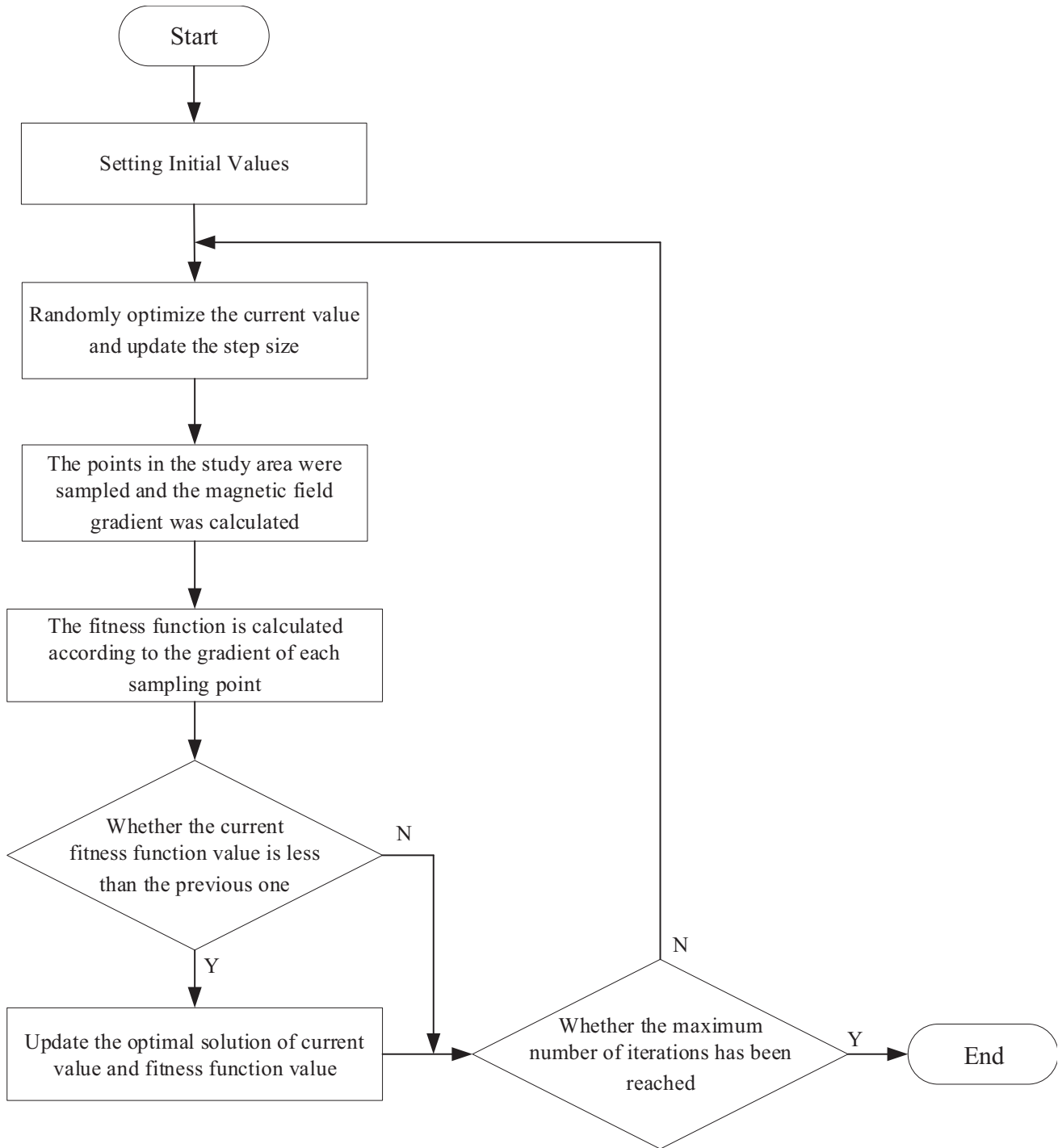


**Figure 3.** Flowchart of current excitation parameter optimization.

and 200 A. Therefore, the multi-coil structure can effectively reduce the current excitation. At the same time, the smaller fitness function of the coil structure is, the higher the uniformity of the gradient magnetic field is in the imaging region.

In this paper, multi-physical field simulation software COMSOL is used to build the above five coil structures. The structure parameters of the coils are shown in Table 2. According to the optimized coil current, the electromagnetic field simulation research is carried out. According to Equation (6), the

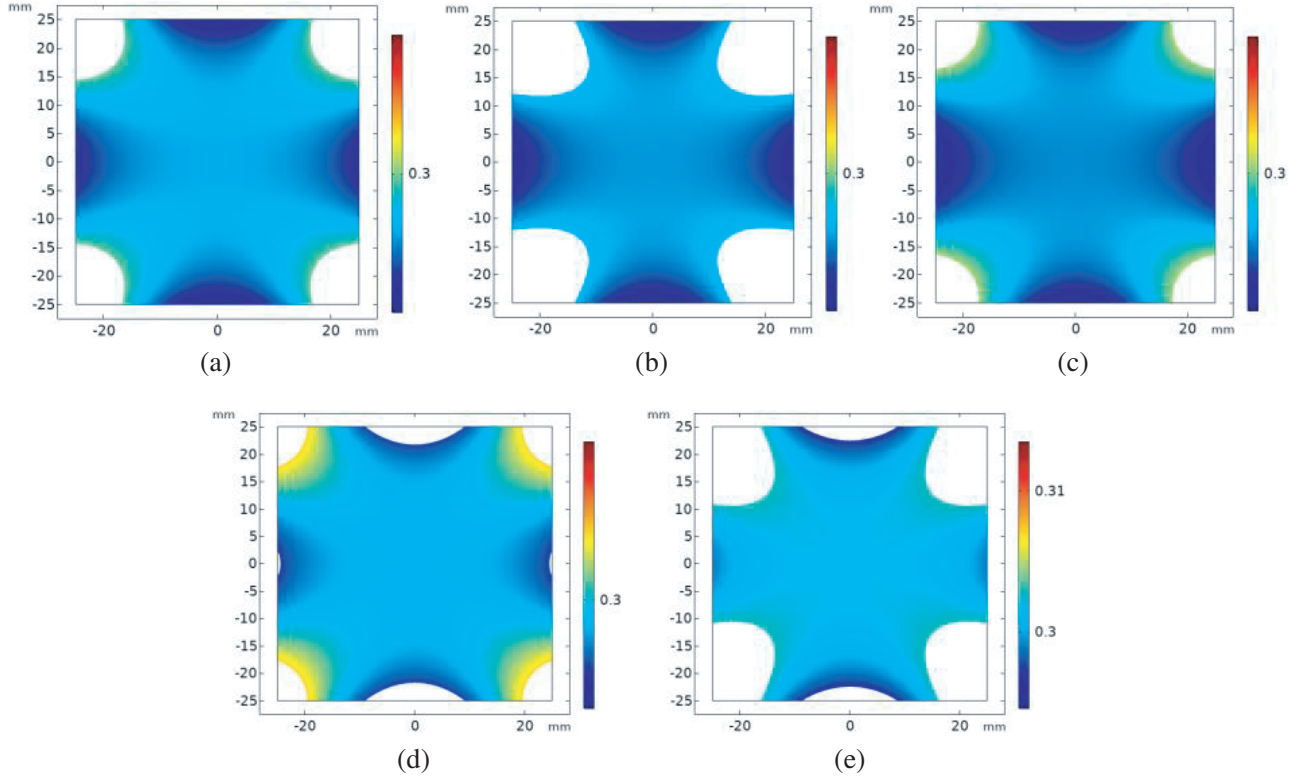
**Table 1.** The optimization results.

	$I1$ (A)	$I2$ (A)	$I3$ (A)	$Fitness$
$R1 = R2 = R3$	157	153	128	0.0004862
$R1 < R2 < R3$	141	161	161	0.0020046
$R1 > R2 > R3$	157	171	178	0.0001441
$a1 = a2 = a3$	102	111	111	0.0007863
Maxwell coils	241			0.0048552

**Table 2.** Multi-coil structure parameters.

	$a1$ (mm)	$a2$ (mm)	$a3$ (mm)	$R1$ (mm)	$R2$ (mm)	$R3$ (mm)
$R1 = R2 = R3$	80.5	95.5	110.5	104	104	104
$R1 < R2 < R3$	80	95	110	86	116	146
$R1 > R2 > R3$	75	90	105	143	113	83
$a1 = a2 = a3$	73.5	73.5	73.5	70	100	130
Maxwell coils				80		

uniformity of five coil structures is calculated. The area where the gradient magnetic field uniformity produced by each coil is less than 1%, shown in Fig. 4. The gradient magnetic field generated by multi-coil structure has higher uniformity and larger uniform area. The magnetic field gradient of 0.3 T/m

**Figure 4.** Magnetic field gradients in different coil structures. (a)  $R1 = R2 = R3$ . (b)  $R1 < R2 < R3$ . (c)  $R1 > R2 > R3$ . (d)  $a1 = a2 = a3$ . (e) Maxwell coil.

is the same as the optimization results, and the correctness of the optimization algorithm design is proved. According to the comprehensive comparison of the excitation current, the uniformity of the gradient magnetic field and the size of the uniform area, we can acquire the conclusion that the gradient magnetic field generated by the 6-coil structure shown in Fig. 2(c) is the optimal one.

### 3.2. Magnetic Simulation Research

According to the previous optimization results, the six-coil structure is as shown in Fig. 2(c). It was selected to establish the numerical model of human breast with the COMSOL to further analyze and study the physical process of the MACT-MI forward problem. The finite element model of MNPs embedded in biological tissue is shown in Fig. 5. Among them, a sphere area with a radius of 20 mm is used to simulate the breast, and the magnetic properties of biological tissues are also ignored. Set the relative permeability to 1, and the inner layer is embedded with a 4 mm radius of the sphere marked by MNPs clusters of human pathological tissue. The electromagnetic parameters of the breast numerical model are shown in Table 3 [20–22]. Since the Maxwell coil and the six-coil structure designed in this paper will generate a zero magnetic field point in its central area [23], the center of the numerical model of the breast is set at (0, 10).

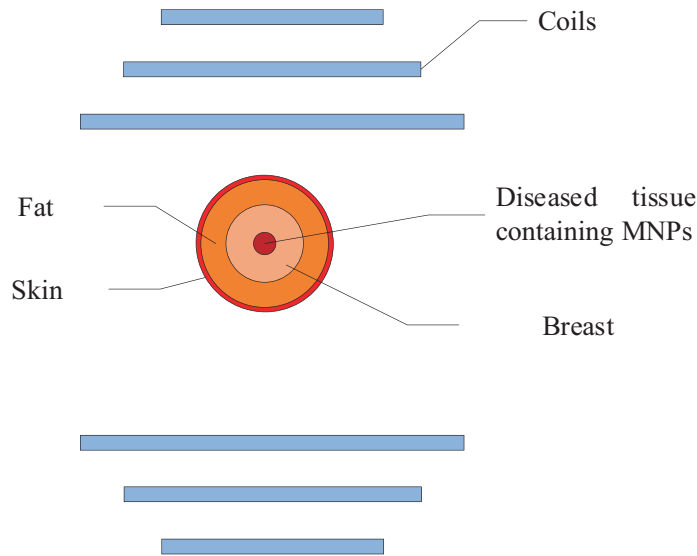


**Figure 5.** Schematic diagram of simulation model.

**Table 3.** Electromagnetic parameters of breast numerical model.

	Dielectric constant $\epsilon$	Conductivity $\sigma$ (S/m)	Relative permeability $\mu$
Skin	39	0.4	1
Fat	5	5e-2	1
Breast	43	0.7	1
Diseased tissue	43	0.7	6

In order to analyze the electromagnetic field instantaneously, the pulse current of multiple coils is passed through. The current value of multiple coils is set as  $I_{1\max} = 157\text{ A}$ ,  $I_{2\max} = 171\text{ A}$ ,  $I_{3\max} = 178\text{ A}$ , and the input current value of the Maxwell coil is set as  $I_{4\max} = 241\text{ A}$ . The coil excitation current waveform is shown in Fig. 6 [10].

The detection target of MNPs combined with pathological tissue was placed under the six-coils and Maxwell coil. Under the excitation of pulse current, MNPs will be acted on by magnetic force.

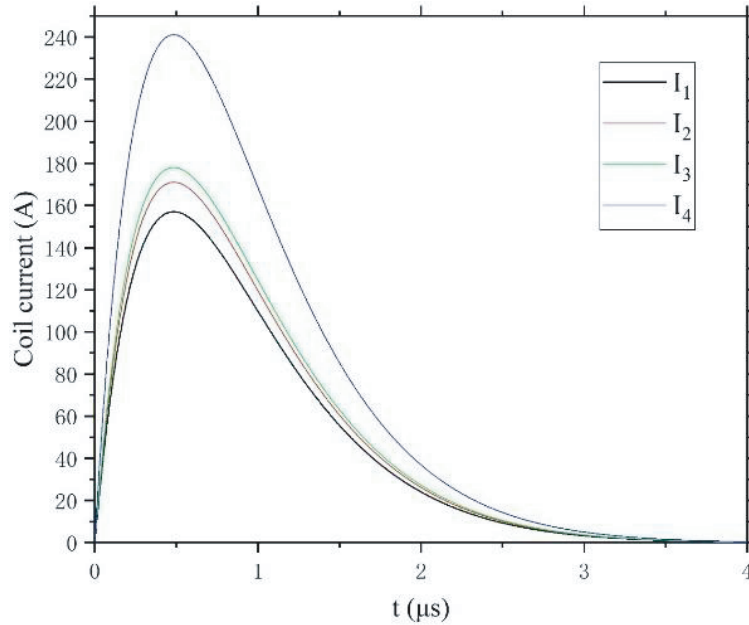


**Figure 6.** The excitation current waveform of the coil.

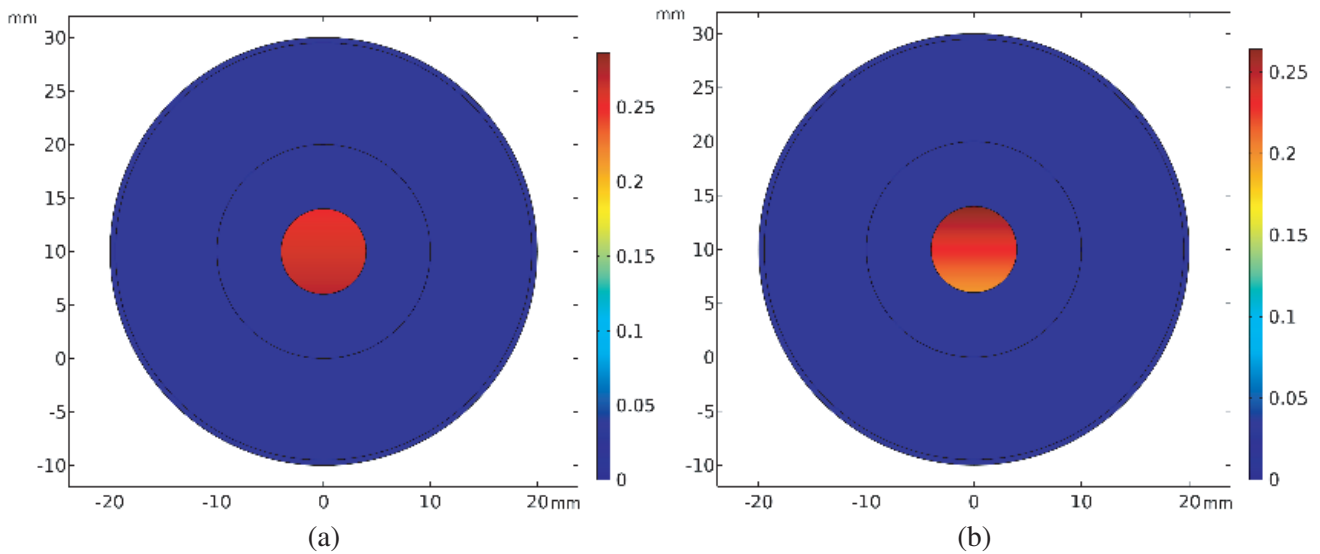


**Figure 7.** Magnetic distribution. (a) Six coils. (b) Maxwell coils.

When the time is  $t = 0.5 \mu\text{s}$ , the magnetic force distribution in the imaging area is shown in Fig. 7. With six-coil structure as the gradient magnetic field excitation system, the magnetic force generated in the biological tissue is more uniform than the Maxwell coil, which can generate stable sound pressure signals. It is more conducive to the signal reception of the ultrasonic transducer and promotes the complete reconstruction of sound source.

### 3.3. Sound Pressure Simulation Study

Furthermore, in order to study the change law of sound pressure in the MACT-MI imaging region under multi-coil excitation, the magneto-acoustic coupling field of the breast numerical model was solved

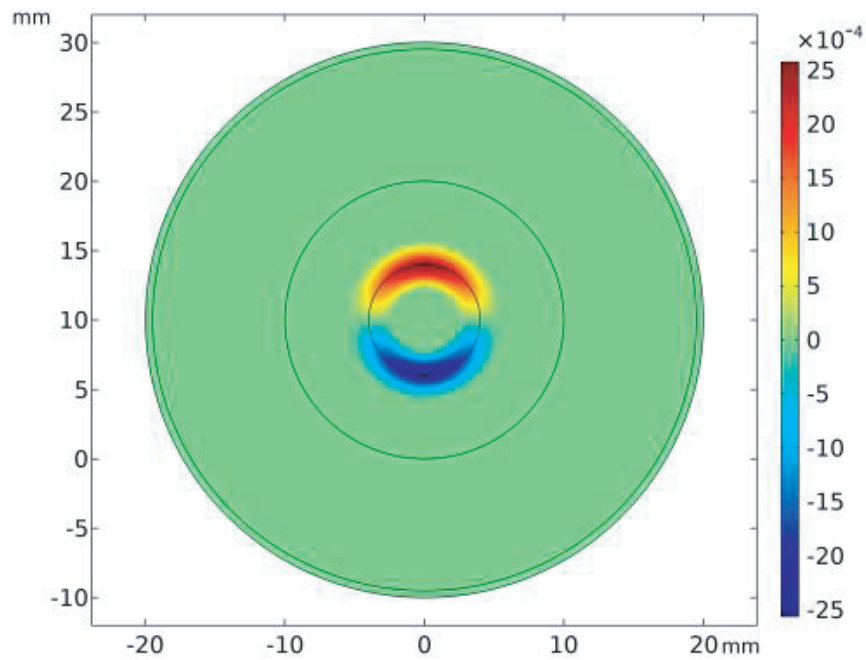


**Figure 8.** Sound pressure distribution.

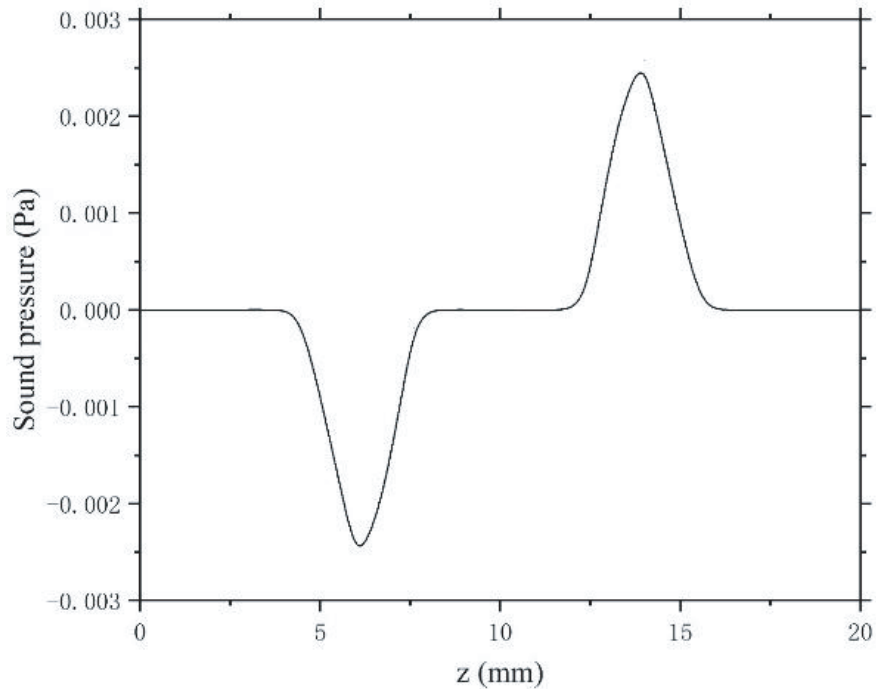


**Figure 9.** Sound pressure curve.

instantaneously according to the simulation results of the electromagnetic field. When  $t = 1.2 \mu\text{s}$ , the distribution of sound pressure in the imaging region is shown in Fig. 8. Under the excitation of multiple coils, the sound pressure in the imaging region is mainly distributed around the upper and lower edges of the cluster. The sound pressure is symmetrical from top to bottom, but the direction is opposite, because the lesion tissues labeled by MNPs have characteristics similar to dipole sound sources.

In order to study the law of acoustic pressure change with the spatial location, as shown in Fig. 8, we intercept the line segment AB between and 20 mm on the  $z$  axis zone. Under the incentive of the multi-coil structure, sound pressure distribution on the cutting line AB is shown in Fig. 9. From the point of  $z$  direction, sound pressure peak appeared in the measured target boundaries, namely the distance between the two positive and negative peaks in the figure of 8 mm. The ultrasonic transducer can be used to detect the sound pressure data at the boundary of the imaging target, and the inverse problem imaging algorithm can be used to reconstruct the sound source.

#### 4. CONCLUSION

In this paper, the current value of Maxwell coil and multi-coil structure is optimized by using the Beetle Antennae Search algorithm, and the gradient magnetic fields generated by the Maxwell coil and multi-coils are compared. The lesions labeled by MNPs are placed in the gradient magnetic field generated by multi-coils to calculate the magnetic force and sound pressure of MACT-MI. The simulation results show that: (1) Compared with the Maxwell coil structure of the traditional MACT-MI system, the multi-coil structure can effectively reduce the current excitation and provide a higher uniformity and a larger gradient magnetic field in the uniform area. (2) The magnetic force generated by the multi-coil structure acting on MNPs is more uniform, and the magnetoacoustic signal of the lesion tissue boundary can be clearly distinguished by the sound pressure curve.

In this paper, through simulation analysis, it is proved that multi-coils can generate more effective gradient magnetic field by using small current excitation, which is more beneficial to the reconstruction of sound source. However, the research in this article still has some shortcomings. For example, the influence of coil inductance is not considered in the construction of multiple coils. No physical objects are constructed to further verify the model. In addition, the MACT-MI experimental system with matrix coil structure can also be studied.

#### ACKNOWLEDGMENT

This research was supported by the Natural Science Foundation of Liaoning Province (No. 2019-ZD-0039) and the Basic Scientific Research Project of Liaoning Education Department (No. LJ2020JCL003).

#### REFERENCES

1. Guo, Y. and X. Fan, "Ultrasound molecular imaging: Present situation and future," *Journal of the Third Military Medical University*, Vol. 36, No. 01, 6–10, 2014.
2. Pysz, M. A., S. S. Gambhir, and J. K. Willmann, "Molecular imaging: Current status and emerging strategies," *Clinical Radiology*, Vol. 65, No. 7, 0–516, 2010.
3. Chu, C. C. And G. Liu, "Hot spots and challenges of magnetic nanomolecular imaging probe," *Science & Technology Review*, Vol. 36, No. 22, 89–97, 2018.
4. Oh, J., M. D. Feldman, J. Kim, et al., "Detection of magnetic nanoparticles in tissue using magneto-motive ultrasound," *Nanotechnology*, Vol. 17, No. 16, 4183–4190, 2006.
5. Mehrmohammadi, M., J. Oh, S. Mallidi, et al., "Pulsed magneto-motive ultrasound imaging using ultrasmall magnetic nanoprobe," *Molecular Imaging*, Vol. 10, No. 2, 2011.
6. Hu, G. and B. He, "Magnetoacoustic imaging of magnetic iron oxide nanoparticles embedded in biological tissues with microsecond magnetic stimulation," *Applied Physics Letters*, Vol. 100, No. 1, 484, 2012.
7. Bringout, G. and T. M. Buzug, "Coil design for magnetic particle imaging: Application for a preclinical scanner," *IEEE Transactions on Magnetism*, Vol. 51, No. 2, 1–8, 2015.
8. Yan, X.-H., Y. Zhang, and G.-Q. Liu, "Simulation research on effect of magnetic nanoparticles on physical process of magneto-acoustic tomography with magnetic induction," *Chinese Physics B*, Vol. 27, No. 10, 104302, 2018.

9. Hamanaga, S., T. Yoshida, T. Sasayama, et al., "Three-dimensional detection of magnetic nanoparticles using a field-free line with weak field gradient and multiple pickup coils," *Japanese Journal of Applied Physics*, Vol. 58, No. 6, 061001.1–061001.6, 2019.
10. Shi, X., G. Liu, X. Yan, et al., "Simulation research on magneto-acoustic concentration tomography of magnetic nanoparticles with magnetic induction," *Computers in Biology and Medicine*, Vol. 119, 103653, 2020.
11. Yan, X., Z. Xu, W. Chen, et al., "Implementation method for magneto-acoustic concentration tomography with magnetic induction (MACT-MI) based on the method of moments," *Computers in Biology and Medicine*, Vol. 128, 104105, 2021.
12. Sun, X., D. Hao, and D. Peng, "Analysis of magnetic field and magnetic gradient of Maxwell coil," *Magnetic Materials and Devices*, Vol. 51, No. 02, 16–19, 2020.
13. Mihailescu, B., M. N. Velcea, and I. Plotog, "Comparative assessment of maxwell and Helmholtz coils magnetic field for biotechnological applications," *IEEE International Symposium for Design and Technology in Electronic Packaging, SIITME 2015*, IEEE, 2015.
14. Wang, J. and H. Zhou, "Design method of permanent magnet MRI gradient coils," *Chinese Journal of Medical Devices*, Vol. 33, No. 03, 188–192, 2009.
15. Jin, D., D. F. Cheng, and Y. Z. Wang, "Design of a magnetic gradient coil with high uniformity," *Applied Mechanics & Materials*, Vol. 556–562, 1865–1869, 2014.
16. Song, X. C., "Comparison of magnetic field distribution and uniformity of helmholtz coils and Maxwell coils," *Magnetic Materials and Devices*, Vol. 47, No. 05, 16–18+77, 2016.
17. Jiang, X. and S. Li, "BAS: Beetle antennae search algorithm for optimization problems," *International Journal of Robotics and Control*, Vol. 1, No. 1, 2017.
18. Jiang, X. and S. Li, "Beetle Antennae Search without Parameter Tuning (BAS-WPT) for multi-objective optimization," 2017.
19. Wang, Q., S. Wei, Z. Wang, and W. Yang, "Optimization design of matrix gradient coil based on particle swarm optimization and genetic algorithm," *Journal of Spectrum*, Vol. 36, No. 04, 463–471, 2019.
20. Bellizzi, G., O. M. Bucci, and I. Catapano, "Microwave cancer imaging exploiting magnetic nanoparticles as contrast agent," *IEEE Transactions on Bio-medical Engineering*, Vol. 58, No. 9, 2528, 2011.
21. Bevacqua, M. T. and R. Scapaticci, "A compressive sensing approach for 3D breast cancer microwave imaging with magnetic nanoparticles as contrast agent," *IEEE Transactions on Medical Imaging*, Vol. 35, No. 2, 665, 2016.
22. Song, J., Z. Zhao, J. Wang, et al., "Evaluation of contrast enhancement by carbon nanotubes for microwave-induced thermoacoustic tomography," *IEEE Transactions on Biomedical Engineering*, Vol. 62, No. 3, 930–938, 2015.
23. Yan, X., Y. Pan, W. Chen, et al., "Simulation research on the forward problem of magnetoacoustic concentration tomography for magnetic nanoparticles with magnetic induction in a saturation magnetization state," *Journal of Physics D: Applied Physics*, Vol. 54, No. 7, 075002 (10pp), 2021.